ADVANCES IN ATMOSPHERIC SCIENCES, VOL. 34, FEBRUARY 2017, 258–271

• **Original Paper** •

Analysis of a Mesoscale Convective System that Produced a Single Sprite

Jing YANG*[1,2], Gaopeng LU[1,2], Ningyu LIU[3], Haihua CUI[4], Yu WANG[5], and Morris COHEN[6]

[1]*Key Laboratory of Middle Atmosphere and Global Environment Observation, Institute of Atmospheric Physics, Chinese Academy of Sciences, Beijing* 100029*, China*

[2]*Collaborative Innovation Center on Forecast and Evaluation of Meteorological Disasters, Nanjing University of Information Science and Technology, Nanjing* 210044*, China*

[3]*Geospace Physics Laboratory, Physics and Space Sciences Department, Florida Institute of Technology, Melbourne, FL* 32901*, USA*

[4]*Hebei Province meteorological Bureau, Shijiazhuang* 050000*, China*

[5]*State Grid Electric Power Research Institute, Wuhan* 430074*, China*

[6]*School of Electrical and Computer Engineering, Georgia Institute of Technology, Atlanta, GA* 30332*, USA*

(Received 8 April 2016; revised 26 July 2016; accepted 8 October 2016)

ABSTRACT

Sprites are brief optical emissions occurring above thunderstorms. Features of sprites and their parent thunderstorms and lightning activities have been studied by many researchers. Here, we report a single sprite recorded over a mesoscale convective system during its life cycle in Northeast China. The results show that the sprite might have been a dancing one, with a 20 km horizontal displacement from its parent cloud-to-ground flash (CG) and a 38 ms time delay; all the sprite elements occurred during the continuing current process of the parent flash. The peak current of the parent CG was the largest during the almost one-hour time window containing the sprite, and the absolute values of all the negative flashes were smaller than 100 kA during the same time period and did not produce sprite. The sprite did not occur during the time period in which the maximum area of the thunderstorm reached. The occurrence of sprite corresponded well with the decay of the thunderstorm convection, and no significant relationship between the occurrence of sprite and the increase in the 30–35 dBZ and 35–40 dBZ interval was found. The large wind gradient in the 8–12 km region of the thunderstorm may have played an important role in the sprite production.

Key words: sprite, mesoscale convective system, Doppler radar, lightning, magnetic field

Citation: Yang, J., G. P. Lu, N. Y. Liu, H. H. Cui, Y. Wang, and M. Cohen, 2017: Analysis of a mesoscale convective system that produced a single sprite. *Adv. Atmos. Sci.*, **34**(2), 258–271, doi: 10.1007/s00376-016-6092-0.

1. Introduction

Transient luminous events (TLEs) are brief optical emissions that occur above thunderstorms, and sprites are one of the dominant members in the TLE family. Since the first image serendipitously captured by Franz et al. (1990), ground- and aircraft-based observations and theoretical studies of TLEs have been carried out all over the world (Sentman et al., 1995; Lyons, 1996; Pasko et al., 1997; Stanley et al., 2000; Neubert et al., 2001; Su et al., 2002; Chern et al., 2003; Cummer and Lyons, 2005; Ganot et al., 2007; Kuo et al., 2007, 2009; Williams et al., 2007, 2012; Liu et al., 2012; Sonnenfeld and Hager, 2013; Yang et al., 2013a, b, 2015; Liu et al., 2015a, b, c; Sato et al., 2015, 2016). Among the known types of TLEs, sprites are most commonly observed in ground observations, and the two main morphologies of sprites take the shape of "column" and "carrot"; in addition to column and carrot sprites, "firework" sprites (Su et al., 2002), "Jellyfish" sprites and "dancing" sprites (Lyons, 1994, 1996) have also occasionally been reported, demonstrating a wide variety in their morphologies.

Although observations of dancing sprites can be occasionally found in the literature (Lyons, 1994, 1996; Winckler et al., 1996; Hardman et al., 2000), their formation mechanism is not well understood. The analysis by Lu et al. (2013), with several cases observed over a mesoscale convective system (MCS) in the central United States, suggested that dancing sprites could be produced either by discrete strokes in positive cloud-to-ground (CG) flashes, or by brief current surges during the continuing current of a +CG stroke (Li et al., 2008). Both mechanisms could lead to a brief intensification of the lightning-induced electrostatic field responsible for sprite production (Pasko, 2007). However, in order to formulate a general mechanism for the occurrence of multiple sprite elements at different times during a lightning flash,

* Corresponding author: Jing YANG
Email: yangj@mail.iap.ac.cn

more observations of dancing sprites are needed. Such observations will help us to understand their morphology and association with the dynamic structure of parent lightning flashes and thunderstorms.

Numerous observations have shown that if, an MCS produces a sprite, it will also produce many others, and the sprites usually occur in cluster (Sentman et al., 1995; Lyons, 1996; Hardman et al., 2000; Pinto et al., 2004; Cummer et al., 2006; van der Velde et al., 2006; Yang et al., 2008, 2013a, 2015; Soula et al., 2009, 2015; Lu et al., 2013). Characteristics of sprites and their underlying thunderstorms and lightning activities have been reported by many researchers. In the present study, we report an analysis of an MCS thunderstorm that produced only one sprite during its entire life cycle. Compared to a typical sprite-producing MCS, i.e., one that produces many sprites, the limited sprite-producing thunderstorm analyzed here may be scientifically interesting, because it probably presents fairly unique properties.

2. Data description

Sprite observations have been conducted in Shandong Province since 2007 (Yang et al., 2008). In 2014, a new station was established at Xinglong Observatory [(40°23′39″N, 117°34′35″E); 960 m above sea level], Hebei Province. At this location, no high buildings exist in the field view of the camera, and the environment is clear without background light at night (see the picture in the lower-right corner of Fig. 1), which is very suitable for TLE observations. The observation system installed at this station includes a Watec 902H2 Ultimate low-light-level video camera (equipped with a Computar 3.6 mm/F1.4 TV lens) with minimum illumination of 0.0001 Lux, and the camera can record static images at a rate of 25 frames per second (or 50 interlaced fields per second). Since we used a fixed short focal length lens, the field of view of the observation system was comparatively large at about 100° (horizontal) ×71° (vertical) (obtained by using the background star field analysis method), ensuring the camera could cover the entire range of a thunderstorm.

The lightning characteristics were obtained from a local lightning detection network as well as the World Wide Lightning Location Network (WWLLN), both of which use very low frequency (VLF, 3–30 kHz) radio receivers. Lightning strokes radiate intense impulsive energy at VLF, which propagate globally and efficiently by reflection from the ground and lower ionosphere (70–85 km altitude). A network of receivers can therefore geolocate and characterize lightning over large areas. WWLLN is a network of more than 50 globally-distributed antennas, one of which is located at the Institute of Atmospheric Physics, Chinese Academy of Sciences (distributed by the University of Washington in Seattle) (Pan et al., 2009; Abarca et al., 2010; Bovalo et al., 2014). WWLLN provides global maps with lightning locations updated every 10 minutes and is available as a historical database. Although the detection efficiency (a few percent) is relatively low, it is nonetheless useful for locating the electri-

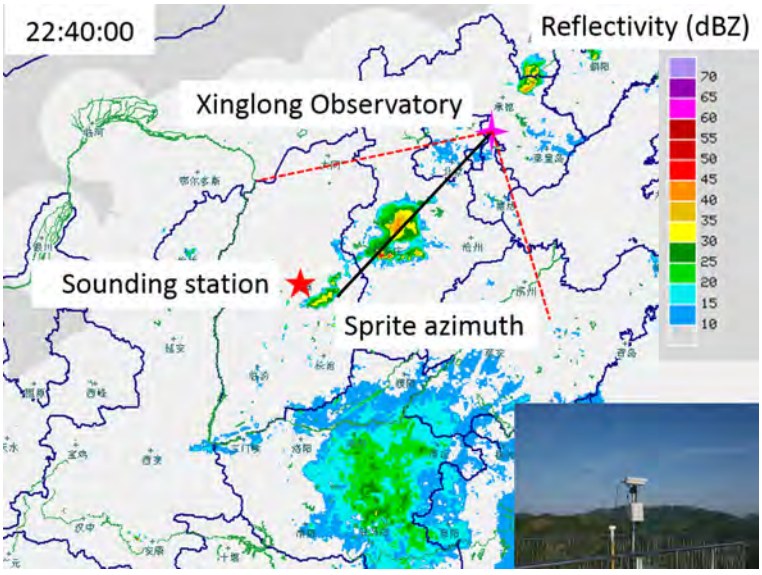

Fig. 1. Radar reflectivity of the thunderstorm that produced the sprite. The thunderstorm was in the detection range of Shijiazhuang radar [(38.352°N, 114.712°E); 134.8 m above sea level]. The black line (labeled "sprite azimuth" in the figure) is the sprite azimuth in the first two fields in Fig. 2. The two dotted red lines are the camera's field of view. The camera's location at Xinglong Observatory is marked by a pink star on the map. The sounding station is marked by a red star. The camera and GPS antenna used in the observation are shown in the photograph in the lower-right corner of the figure.

cal activity center of a thunderstorm.

A set of receivers set up locally uses combined time-of-arrival and magnetic-direction-finding technology (Cummins et al., 1998), and geolocates a much higher fraction of lightning around the observation site. The detection efficiency and location error of the local lightning detection network are about 92% and 760 m, respectively (Zhang et al., 2014). Data from both WWLLN and the local detection network were used for characterizing the lightning characteristics (location, type, peak current, etc.) in sprite-producing thunderstorms of particular interest. Since a lightning flash may contain several strokes, individual strokes were grouped into flashes by associating all strokes with algorithm 1 s and 10 km (van der Velde et al., 2007).

In addition, a broadband VLF magnetic field sensor (500 Hz to 47 kHz), described by Cohen et al. (2010), is located in Dongying, which is only 15 km from the coast of the Bohai Sea. The system consists of a pair of magnetic air-core loop antennas to record two horizontal components of the magnetic fields emitted by lightning discharges. The receiver is sensitive enough to detect even small lightning strokes from many thousands of kilometers away, and is GPS synchronized with a better than 100 ns accuracy. Having access to VLF data allowed us to go beyond what is typically provided by lightning detection networks, because we captured the complete radio signature of the lightning stroke, which is typically thrown away by lightning detection networks after the stroke has been geolocated. Having the radio signature helped us infer the discharge polarity, the discharge process, the vertical current moment and the time-integrated charge moment change (CMC) of TLEs and lightning (Cummer and Lyons, 2005; Lu et al., 2013).

The evolution and structure of the thunderstorm were examined using observations from a Doppler radar located in Shijiazhuang [(38°21′7″N, 114°42′43″E); 134.8 m above sea level], Hebei Province. The radar used in this study was a WSR-98D S-band Fully Coherent Doppler Weather radar, and the radar data were updated every six minutes (Yang et al., 2013a, 2013b). The radar has many features, including state-of-the-art computerized control, 24-h operational capability, real-time monitoring, real-time calibration, and high accuracy and reliability. The development of the sprite-producing thunderstorm during most of its lifetime was located in the radar scanning range (for accuracy, the 230-km scanning range was used, with a resolution of about 1 km).

Atmospheric sounding data were downloaded from http://weather.uwyo.edu/upperair/sounding.html. The data are provided twice daily [0000 and 1200 UTC (Local Standard Time, LST = UTC + 8 h), and the time used in this paper is local except when otherwise noted]. Data from the Taiyuan sounding station [station number 53772; (37.78°N, 112.55°E)] were used in this study. Although the radiosonde data accuracy were limited, being unable to reveal the dynamical structures inside or near thunderstorms, they nevertheless provided information on the large-scale environment in which a thunderstorm developed.

3. Analysis and results

3.1. *Sprite image characteristics*

The sprite was recorded at 2244:01 LST (1444:01 UTC) on 14 August 2014, with a 38 ms delay from its parent CG, over a summer thunderstorm southwest of the observation site. The sprite azimuth, the sprite-producing thunderstorm, the location of the sounding station, and Xinglong Observatory where the camera was located, are shown in Fig. 1.

Figure 2 shows the sprite image captured by the low-light-level imaging system. The recorded sprite lasted three fields and the total duration was about 60 ms. A strong bright center is clearly visible in Fig. 2a, indicating it was a typical carrot-shape sprite. The images show that the sprite was a simple case, with only two elements appearing in different frames. The left-hand column in Fig. 2 shows that the first element of the sprite occurred in Field 1 and then decayed as shown in Field 2, and its location did not change during the evolution in these two fields. The sprite element in Field 3 occurred directly after the previous sprite element, with a horizontal displacement (jumped left), and then disappeared. The sprite evolution was similar to that of dancing sprites reported in the literature (Lyons, 1996; Hardman et al., 2000; Lu et al., 2013), so far as some sprite elements were also observed to decay as other new elements formed, and the new elements were often laterally displaced from the old ones. Since there were only two sprite elements, it is hard to present a time-integrated image to show how the elements were aligned in space and time [see the work of Hardman et al. (2000)]. Therefore, we cannot be totally sure that the observed sprite was a dancing one. However, because the later sprite element was horizontally displaced from previous ones, it was quite likely a dancing sprite.

Lyons (1994) and Winckler et al. (1996) showed that dancing sprites appear sequentially over lateral distances of up to 200 km. By comparing the data from the local lightning detection network and that of WWLLN, the parent CG of the sprite was found, and the distance between the parent CG and the camera was calculated to be about 298 km. Since there was only one observation station, the sprite elements in Fig. 2 could not be triangulated. In order to simplify the question, the sprite elements in Fields 1 and 2 (element locations did not change) in Fig. 2a were assumed to occur directly over the parent flash. Figure 2a shows that the sprite element in Field 3 occurred to the left of the previous one in Fields 1 and 2. By combining the information on the location of the parent CG, the camera field of view, and the elevation of the observation site, the sprite extension and lateral displacement could be estimated using the method mentioned in Hsu et al. (2003) and Yang et al. (2008).

The results showed that the estimated lateral displacement (in this case, it was also the horizontal dimension of the sprite) between the sprite elements in Field 1 (or Field 2) and those in Field 3 was approximately 7.3 km. The actual displacement would be larger if the locations of the elements could be triangulated. Compared with the results reported by Lyons (1994) and Winckler et al. (1996), the lateral displace-

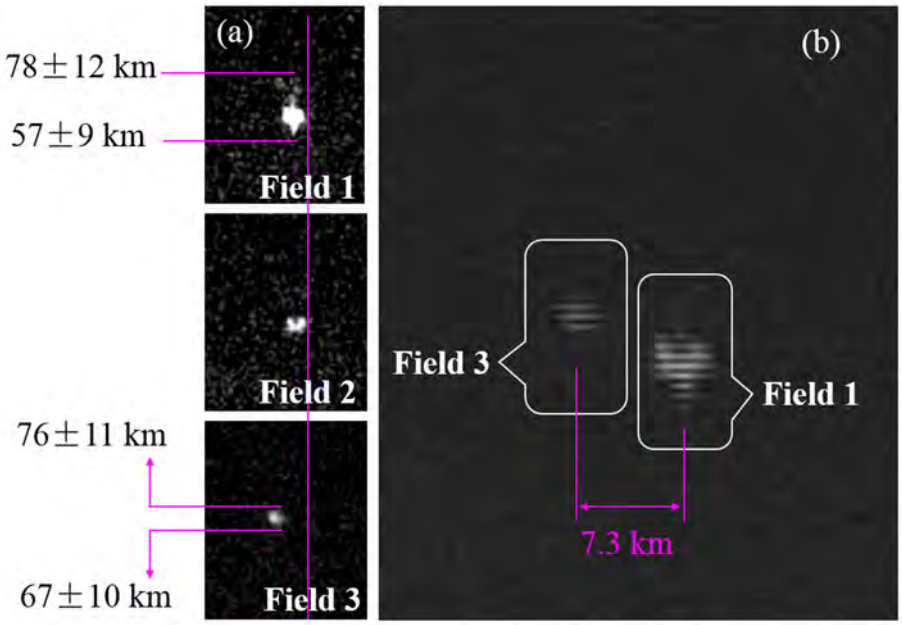

Fig. 2. Sequential images of the sprite. (a) Sprite sequential images (contrast enhanced), numbered as Field 1, Field 2 and Field 3. Since the camera's field of view at this station is comparatively large [100° (horizontal) ×71° (vertical)], the sprite appears small even when the images are enlarged. The sprite's dancing feature (jump to the left of the pink vertical line) is clearly shown. (b) Images (no contrast enhancement) of the sprite elements in Fields 1 and 3.

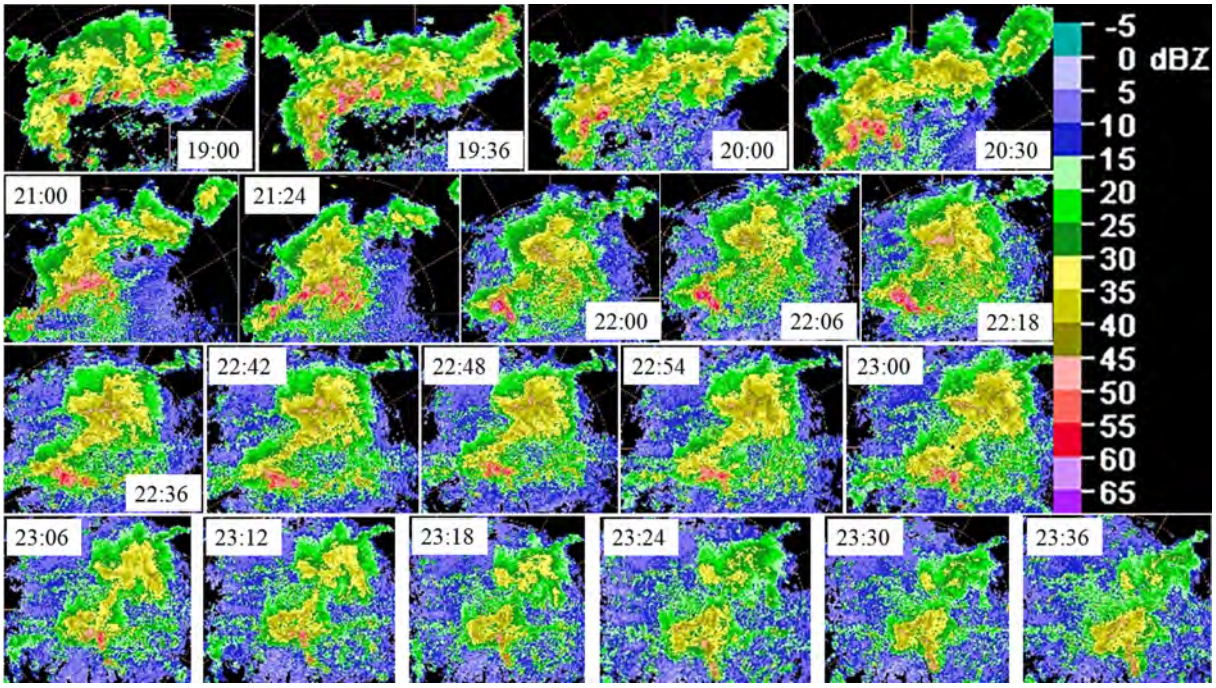

Fig. 3. Composite radar reflectivity evolution of the sprite-producing thunderstorm. The sprite was recorded at 2244:01 LST 14 August 2014.

ment in the present study is small. The small displacement may have resulted from the fact that the sprite consisted of only two elements at different times—far fewer than in Lyons (1994), Winckler et al. (1996), and Hardman et al. (2000).

On the other hand, the lateral displacement of the sprite may also have been constrained by the thunderstorm edge. Indeed, the displacement would have been 9.2 km and 4.8 km, respectively, if we had considered the far and near edges

of the storm from the observation site. Even though the horizontal displacement was considered in three dimensions, it was still much smaller than that in Lyons (1994) and Winckler et al. (1996). It is reasonable to infer that the comparatively small parent thunderstorm (around 140 km in the east–west and south–north directions) may not have had the ability to produce a sprite with a lateral displacement larger than the thunderstorm size. The vertical extension of the sprite was estimated using the method mentioned above, and it was found that the edges of the sprite in Field 1 were about 57 ± 9 km and 78 ± 12 km, respectively, assuming a 50-km variation of the parent CG location. Compared with other results, the vertical extension of the sprite in this study was small, and may to some extent have resulted from the dim image from which the sprite edges were underestimated.

3.2. *Thunderstorm evolution and characteristics*

The Doppler radar images in Fig. 3 show that the sprite-producing thunderstorm developed originally in the intersection of Inner Mongolia Autonomous Region, Shanxi and Hebei provinces at 1400 LST 14 August. The thunderstorm moved to the southeast along the boundary line of Hebei and Shanxi provinces, and was in the scanning range of Shijiazhuang radar at 1500 LST 14 August. At 1900 LST, the thunderstorm was composed of some small strong convective cells with maximum radar reflectivity of 55 dBZ in the front and a trailing stratiform region just behind the convective cells, as shown in Fig. 3. The thunderstorm became more organized and strengthened at 1936 LST (some convective cells could be seen in the trailing stratiform region), and then weakened at 2000 LST. After 2030 LST, some strong convective cells, also with maximum radar reflectivity of 55 dBZ, occurred in the south of the thunderstorm and became stronger and more compact at 2100 LST, and then weakened at 2200 LST. The thunderstorm became even weaker at 2206 LST, as indicated by the decreased area of radar reflectivity (larger than 30 dBZ) (Fig. 4a). After 2206 LST, the overall intensity of the thunderstorm increased a little, as shown by the reflectivity of 45–50 dBZ in the center of the stratiform region (at 2218 LST in Fig. 3, and also indicated by the increased area of 30–40 dBZ in Fig. 4b). After 2300 LST, the thunderstorm weakened rapidly and almost disappeared at 2400 LST 14 August (for brevity, the reflectivity images after 2336 LST are not shown in Fig. 3). The sprite occurred at 2244 LST during the thunderstorm dissipating stage, consistent with previous studies (Lyons et al., 2003; Yang et al., 2013a, b; Soula et al., 2015).

The thunderstorm was an MCS and was in the camera field of view during its whole evolution, but only one sprite was captured during the MCS' life cycle. According to Lyons et al. (2003), summer MCSs are thought to be sprite-productive, and mesoscale convective complexes (thunderstorm area of $\sim 10^5$ km^2) are believed to be the most sprite-productive thunderstorm type. Lyons et al. (2003) mentioned that the area of sprite-producing MCSs (radar reflectivity values $>\sim$10 dBZ) can reach around 20 000 km^2; that is, 20 000 km^2 might be a prerequisite for a probable sprite-producing storm in the High Plains of the United States. Since only one sprite was recorded during the MCS under study, it would be of interest to study the radar reflectivity characteristics before, during and after the sprite event. The evolution of areas of different radar reflectivity were comprehensively analyzed and the results are shown in Fig. 4.

The results show that the thunderstorm area (radar reflectivity $\geqslant$10 dBZ) at 2242 LST (two minutes before the sprite) was around 20 398 km^2 (Fig. 4a), consistent with the value (15 000–20 000 km^2) obtained in Lyons et al. (2003), but much smaller than that of most sprite-productive thunderstorms ($\sim 10^5$ km^2) (Lyons, 1996; Lyons et al., 2003). The maximum area ($\geqslant$10 dBZ) of the thunderstorm during its evolution was about 23 948 km^2 (Fig. 4a), which is smaller than the result of $\sim 10^5$ km^2 reported by Lyons et al. (1996, 2003), São Sabbas and Sentman (2003) and Soula et al. (2009), indicating that this sprite-producing thunderstorm was comparatively small. It should, however, be noted that the thunderstorm areas reported by São Sabbas and Sentman (2003) and Soula et al. (2009) were obtained using infrared weather images and, therefore, the results could be quite uncertain.

Based on two sprite-producing thunderstorms, Soula et al. (2009) found that the maximum area of the storm was reached during the sprite production period. However, the radar reflectivity area in this study reached a maximum value at 2100 LT, about 1 hour and 44 mins before the sprite occurrence (Fig. 4a). After 2100 LST, the thunderstorm area decreased to a low value at 2206 LST. After 2206 LST, the overall intensity of the thunderstorm increased a little, as shown by the increase in the area of reflectivity larger than 30 dBZ (Figs. 4a and b). The area of the 10–30 dBZ reflectivity region at 2218 LST ($\sim$15 488 km^2) was larger than that at 2200 LST ($\sim$14 202 km^2), and did not change much at 2242 LST (two minutes before the sprite) (for brevity, the figure is not shown), but no sprites were recorded from 2218 to 2242 LST. The area of radar reflectivity ($\geqslant$10 dBZ) two minutes before the sprite (2242 LST) was a medium value (not the largest, not the smallest) with respect to the entire evolution of the thunderstorm.

Both the thunderstorm as a whole and the convective cores in the southwest of the thunderstorm became weaker at 2242 LST; the thunderstorm area also became smaller, and the sprite occurred just two minutes later after 2242 LST. After the sprite, both the thunderstorm strength and stratiform area did not change much (see the evolution of the reflectivity area shown in Figs. 4a and b, plus the radar reflectivity at 2248, 2254 and 2300 LST shown in Fig. 3), but no sprites were recorded. At 2300 LST, the thunderstorm area was a little larger than that in the time window containing the sprite. After 2300 LST, the thunderstorm area decreased rapidly, indicating that the thunderstorm was dissipating quickly at this time, and almost disappeared at 2400 LST.

Soula et al. (2009) showed that sprite production periods correspond well with an increased area of the 35–40 dBZ and 30–35 dBZ ranges. Figure 4b shows that the radar reflectivity with 30–35 dBZ and 35–40 dBZ decreased to its lowest value during the time period shown in the figure, at 2206 LST. Dur-

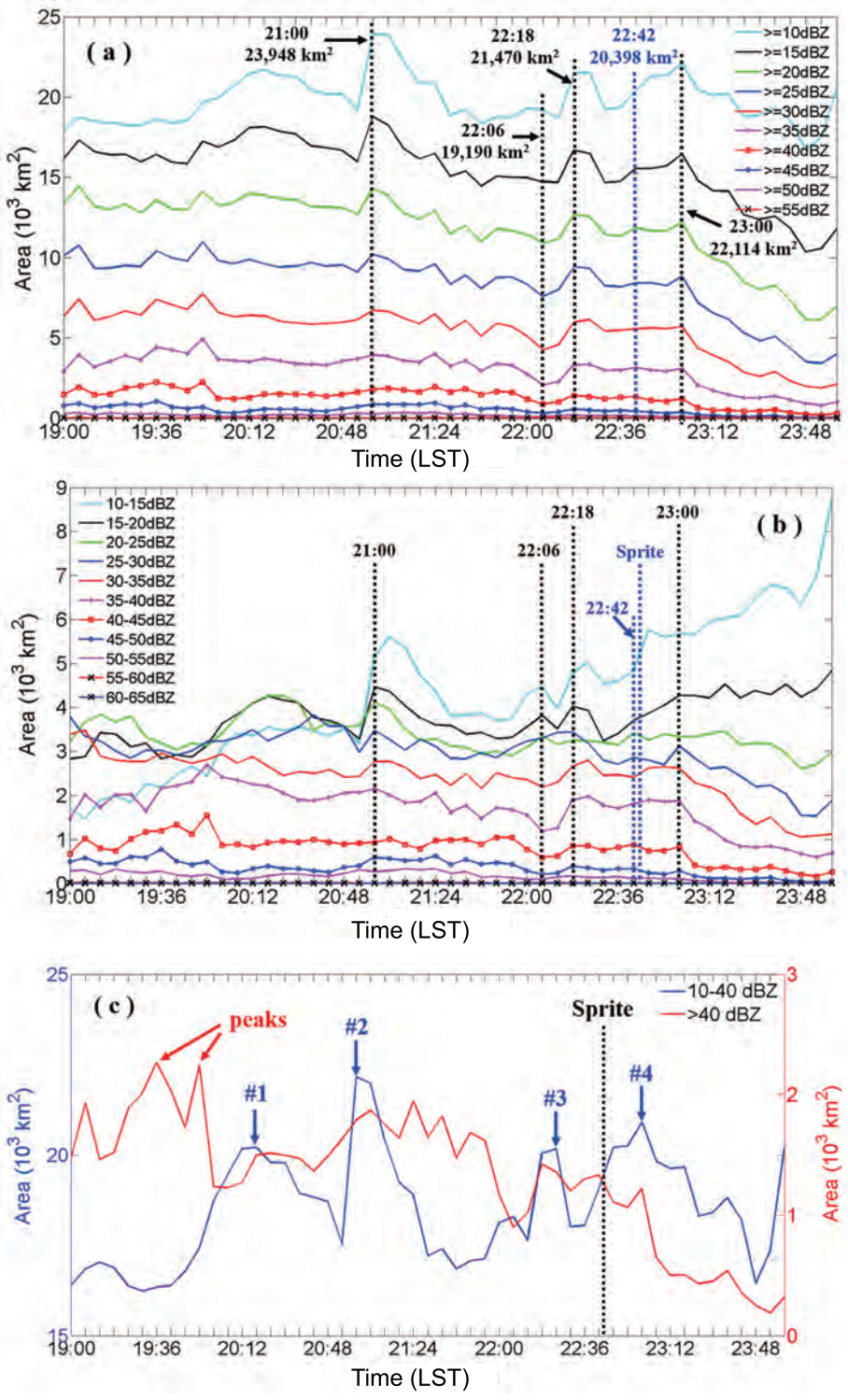

Fig. 4. Areal evolution of different radar reflectivities during the sprite-producing thunderstorm. (a) Areal evolution of radar reflectivity larger than a certain value. (b) Areal evolution of different radar reflectivities. (c) Areal evolution of radar reflectivity with 10–40 dBZ (blue line) and larger than 40 dBZ (red line). The sprite occurrence time is also labeled in the figure.

ing the time window containing the sprite (2218–2300 LST), the area of reflectivity with 30–35 dBZ and 35–40 dBZ did not change much. Therefore, no significant relationship between the sprite and the increase of the 30–35 dBZ and 35–40 dBZ ranges was found in this study.

Most sprites are observed when the area of the stratiform region develops rapidly. However, further analysis, shown in Fig. 4c, indicates that the area of 10–40 dBZ reflectivity

jumped from 17 526 km^2 at 2054 LST to 22 157 km^2 at 2100 LST, but no sprites were recorded. Four large values of area with 10–40 dBZ reflectivity occurred during the observations at night, and are named as #1–#4, respectively. The sprite occurred between peaks #3 and #4, during the time period with an area increase of 10–40 dBZ reflectivity. The maximum area with reflectivity larger than 40 dBZ occurred at 1936 and 1954 LST, respectively, and then totally decreased. The sprite occurred during the decrease of area with strong reflectivity (larger than 40 dBZ). The increase of area with 10–40 dBZ reflectivity and decrease with larger than 40 dBZ reflectivity in the time window containing the sprite shows that the thunderstorm was dissipating, and the sprite production was related to the decay of the convection. The increase of area with 10–40 dBZ reflectivity continued for 24 minutes (from 2236 to 2300 LST), but no other sprites were recorded.

3.3. *Thunderstorm lightning activity*

Figure 5 shows the evolution of the lightning flash rate (flashes per five minutes) from 1900 to 2400 LST obtained from the local lightning detection network. The results show that both negative CGs and positive CGs were in the lower level during the time period containing the sprite. This resulted from the fact that the thunderstorm was in its dissipating stage in that period. The maximum value of negative CGs occurred between 1900 and 2000 LST in the thunderstorm developing stage. There were three large values (labeled #1–#3, and the largest one was about 61.54%) of POP (percentage of positive CG over total CG) that occurred before the sprite, but no sprite was recorded around these time periods.

The POP value when the sprite occurred was about 20%, which was much smaller than the maximum value of 61.54% during the thunderstorm evolution, and was also smaller than in previous studies (Neubert et al., 2005; Soula et al., 2009). The POP value around the time when the sprite occurred was also much lower than that during the sprite time period of an MCS in the same geographical region (Yang et al., 2013a), showing the variety of lightning activity of sprite-producing thunderstorms even in the same geographical region. The POP value reached 100% at the end of the thunderstorm, indicating that only positive CGs occurred at that time.

3.4. *Parent flash and thunderstorm structure*

Both the local lightning detection network and WWLLN detected the ground striking point of the parent CG return stroke, and the two different lightning location systems obtained almost the same location and time, showing that the parent CG was positive with a single return stroke. Results reported by Lu et al. (2013) showed that dancing/jumping sprite events associated with a single lightning flash can be produced either by discrete strokes of the flash, by a single stroke through a series of current surges superposed on an intense continuing current, or by both.

Figure 6 shows the broadband (500 Hz to 47 kHz) radio-frequency magnetic fields recorded at a distance of 400 km. The impulsive signal from the sprite-producing stroke is distinct, with peak magnitude of 2.4 nT. With an empirical relationship based on the estimated iCMC (impulse charge moment change, defined as the product of the charge transferred by the +CG stroke within 2 ms after stroke onset and the original height of the transferred positive charge) from remote sensing of ultra low-frequency (ULF) magnetic fields, a 2-ms ULF magnetic pulse peaking at 1 nT and measured at a distance of 400 km is equivalent to an iCMC of 100 C km (C km means coulomb kilometers, which is the units of the product of charge transfer and the vertical distance over which that charge is transferred) (Lu et al., 2012; Lu et al., 2013). By filtering the magnetic pulse using a low-pass filter with a cut-off frequency of 5 kHz (leaving a 2-ms pulse peaking at about 0.5 nT), we were able to estimate the iCMC to be about 50 C km.

Compared with other studies (Hu et al., 2002; Cummer

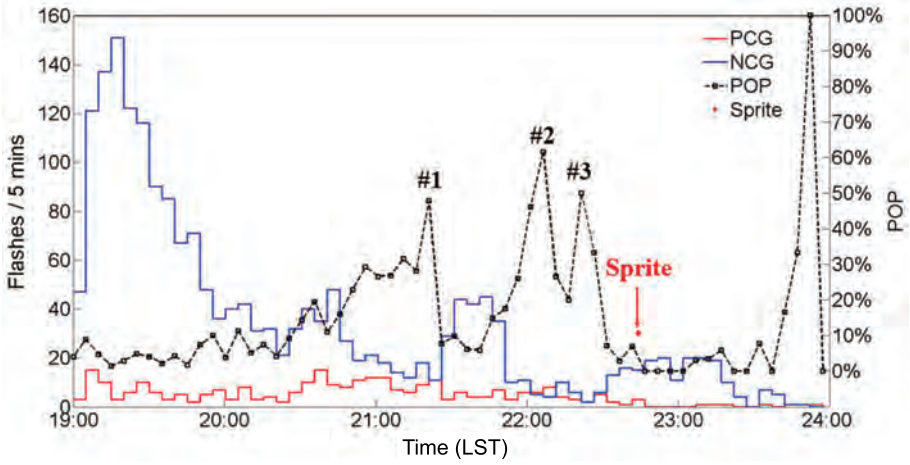

Fig. 5. Flash rate evolution from 1900 to 2400 LST. PCG, NCG, POP and Sprite stand for positive CG, negative CG, the ratio of PCG over total CG and sprite, respectively. The sprite occurrence time is shown in the figure.

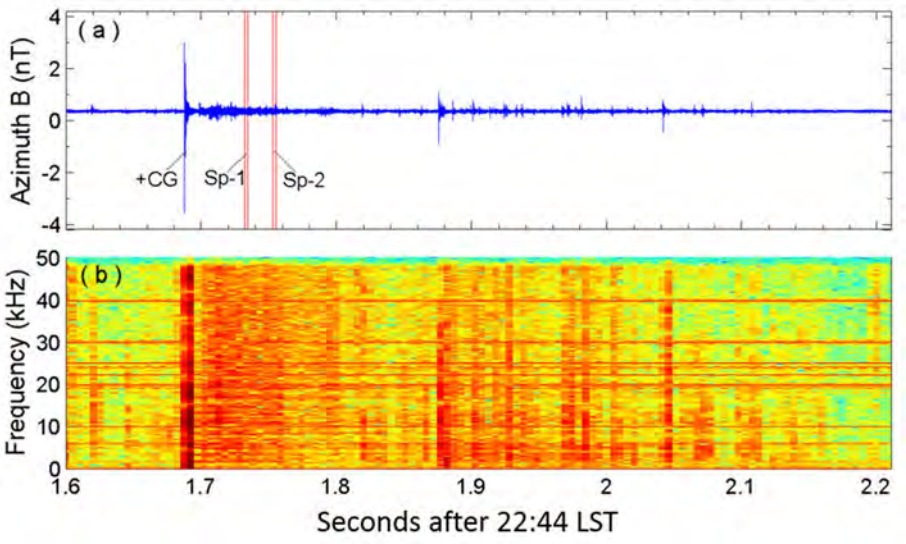

Fig. 6. Broadband lightning signals of the parent CG. The red bars in (a) mark the time windows when the two discrete sprite elements were recorded on the low-light-level video camera.

and Lyons, 2005; Qin et al., 2012), the iCMC value in this study is comparatively low. However, Hu et al. (2002) also showed that the iCMC of parent lightning can be as low as 120 C km, although they did note that the value of 120 C km was probably an exceptional case. It should also be noted that the duration for CMC estimation was about 6 ms in Hu et al. (2002)—significantly longer than the 2 ms in the present study. On the other hand, the iCMC obtained here is higher than the results of Lu et al. (2013), in which the iCMCs (calculated with a duration of 2 ms) of parent flashes could be as low as 28 and 36 C km.

As shown in Fig. 6, the burst of magnetic pulses after the return stroke was indicative of an intense continuing current (with a duration of at least 100 ms), which is generally believed to be responsible for long-delayed sprites (Li et al., 2008; Lu et al., 2013) (the sprite occurred at least 38 ms after the parent stroke in this study); the source of this burst of magnetic pulses could have been the extensive in-cloud progression of negative leaders during the continuing current (Lu et al., 2009). All sprite elements were produced during the continuing current. From the above analysis, it is reasonable to infer that the parent flash in our observation may have belonged to the second case in Lu et al. (2013), although no lightning VHF (very high frequency) radiation source data were available.

In order to clearly show the thunderstorm structure at 2242 LST (two minutes before the sprite event), overlaps of radar reflectivity at different elevations with positive return strokes and negative ones are shown in Fig. 7. The "+" stand for positive strokes and "−" for negative ones. The radar reflectivity at 2236, 2242 and 2248 LST (shown in Fig. 3) did not change much, so the return strokes overlaid in Fig. 7 were chosen in the time period from 2236 to 2248 LST. The result shows that three positive strokes occurred over this time duration. One of them was the parent flash (of the sprite), labeled as CG in Fig. 7, and other two positive strokes are labeled as CG1 and CG2, respectively (as shown in the figure). All the positive strokes (each stroke was actually one positive flash with single stroke) were vertically aligned at the edge of the comparatively strong radar reflectivity region (for the parent CG, see the images with elevation angles of 9.9° and 14.6° in Fig. 7; for CG2, see the image with a 4.3° angle).

Figure 7 shows that the parent CG was very close to the radar station (distance of about 13.88 km), meaning the lower elevation angles of the radar (e.g., 0.5°, 1.5°, 2.4°, 3.4°, 4.3°, 6.0°, 14.6°) could only scan the lower part of the thunderstorm; the top and bottom heights of the radar beam (with an elevation angle of 14.6°) were at about 3.7 and 3.4 km above ground level and at a distance of 14 km. The radar beam, with an elevation angle of 19.5°, can scan a region with heights from 4.6 km to 4.8 km above the ground. Figure 7 shows that, with increasing radar scanning angle, the reflectivity where the parent CG (vertically aligned) was located increased from 20–30 dBZ to about 45 dBZ (elevation angle of 14.6°), and then decreased at the elevation angle of 19.5°. Further analysis of the radar data at this time indicates that the parent CG was vertically aligned with the radar echo top of about 5–8 km (Fig. 8c).

Further analysis of the thunderstorm properties at 2242 LST and return strokes during a longer time span from 2230 LST to 2300 LST is shown in Fig. 8. The return strokes are overlapped with radar reflectivity at 2242 LST with the elevation angle of 0.5°. The results show that only five positive return strokes (including the three positive flashes shown in Fig. 7) occurred during this time period. All of the five positive return strokes were actually five positive flashes; that is, each flash contained only one return stroke. Figure 8a shows that the ground striking points of positive flash 1, flash 3 and flash 4 were located close to the convective region of the thunderstorm. The ground striking point of the parent CG (see images with angles of 9.9° and 14.6° in Fig. 7) and positive flash 2 (see image with angle of 4.3° in Fig. 7) were also

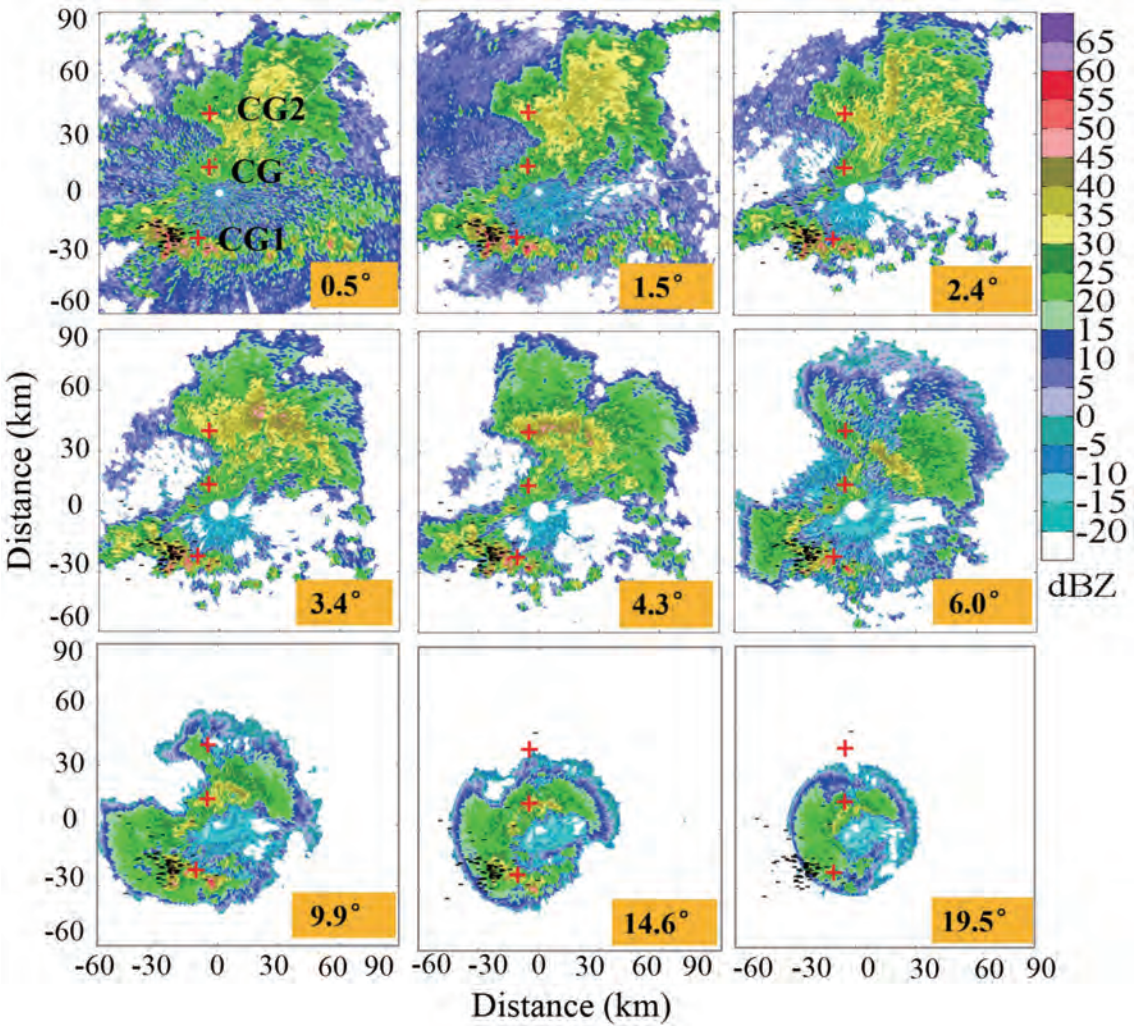

Fig. 7. Overlaps of radar reflectivity at different elevation angles (shown in the figure) at 2242 LST with return strokes during the time period from 2236 to 2248 LST. The "+" stands for positive strokes and "−" for negative ones. The parent flash for the sprite is labeled with "CG" in the figure (the middle "+" in the figure is labeled with 0.5°).

vertically aligned close to the relatively strong reflectivity region.

Vertical cross sections (Fig. 9) are a good representation of the parent thunderstorm structure. The vertical cross section along line AB passing through the parent flash clearly shows the storm vertical structure, indicating that the parent lightning was located in the thunderstorm region with a cloud top at about 6 km. This is broadly consistent with the finding of Lu et al. (2013) that the positively charged region tapped by sprite-producing strokes is located at around 6 km in a thunderstorm during its mature stage. The vertical reflectivity along the sprite element azimuth (lines CD and EF) shows a similar thunderstorm structure. The cloud echo tops obtained from the vertical cross sections are in agreement with the cloud top shown in Fig. 8c.

Figure 10 shows the return stroke peak currents (within 50 km centered at the parent CG location) of positive and negative strokes within half an hour centered at the sprite. The results show that during 30 minutes centered at the sprite, five positive return strokes occurred but the peak current of the parent CG was the largest (131.4 kA). Negative return strokes, which can produce sprites, usually have large peak currents (Li et al., 2012; Boggs et al., 2016), and all the negative return strokes shown in Fig. 10 had peak currents (absolute value) smaller than 100 kA, and were thus not likely to have initiated sprites.

Further analysis of the return stroke peak current distribution during 1900 to 2400 LST 14 August is shown in Fig. 11. The results indicate that the sprite was produced in the thunderstorm dissipating stage. In addition, no lightning flashes occurred about 20 minutes before 2400 LST, showing that the thunderstorm was dying fast at this time. Figure 11 shows that, although the thunderstorm was dominated by negative return strokes, high peak current return strokes were mostly positive strokes. The sprite was produced during a time window (shown in the figure, almost an hour) in which no positive return strokes with peak currents larger than 100 kA occurred, and the absolute values of peak currents of negative

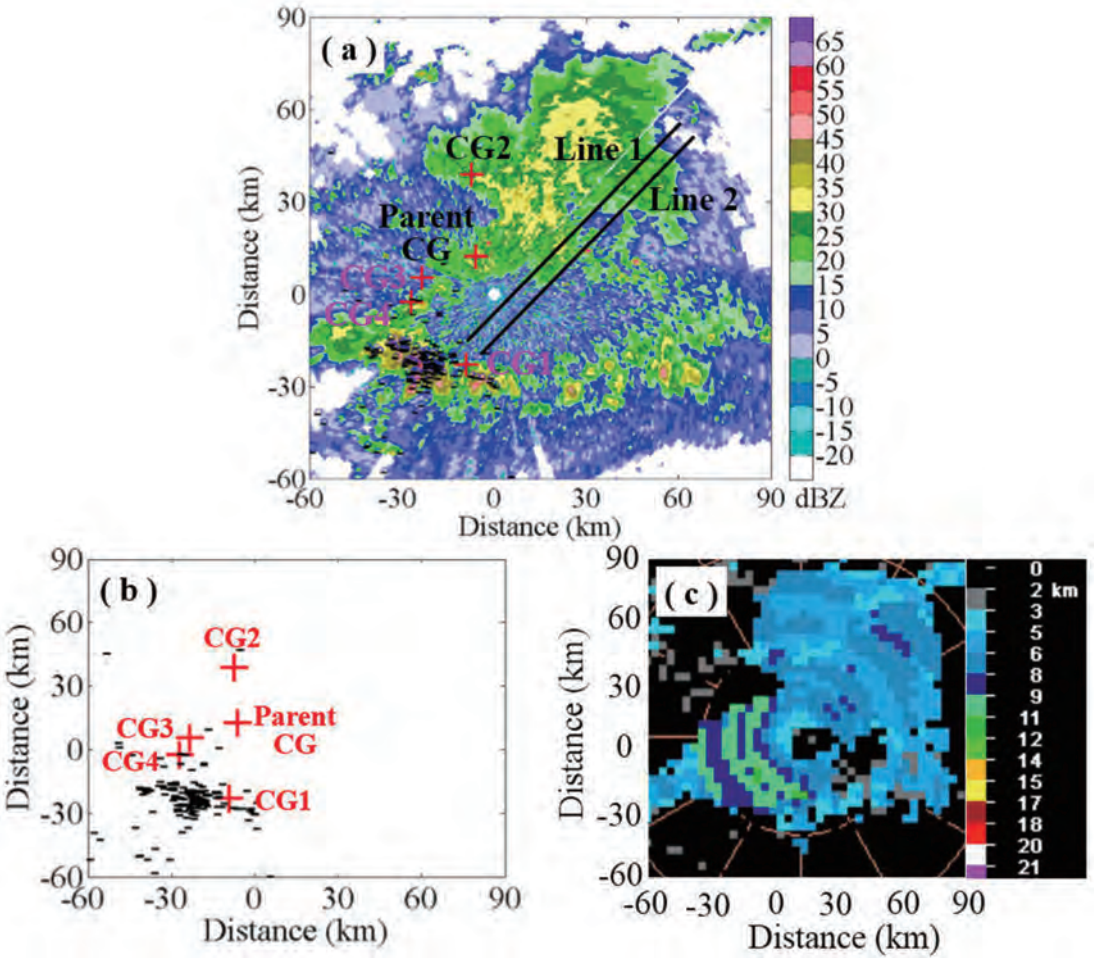

Fig. 8. Thunderstorm structure and lightning activity of the sprite-producing storm. (a) Overlap of radar reflectivity at the 0.5° elevation angle at 2242 LST with return strokes during the time period from 2230 to 2300 LST. The "+" stand for positive strokes and "−" for negative ones. The parent flash for the sprite is marked by "+" and labeled with "Parent CG" in the figure. The black lines 1 and 2 stand for the sprite azimuth in the first two fields and third field in Fig. 2, respectively. (b) Spatial distribution of the same return stroke shown in (a) but without radar reflectivity. (c) Radar echo top at 2242 LST.

strokes were also smaller than 100 kA.

It should also be noted that many positive strokes with large peak currents (larger than 100 kA, with some larger than 200 kA and reaching about 400 kA) occurred during the time period from 1900 to around 2200 LST shown in Fig. 11, but no sprites were recorded. The above result is to some extent consistent with the result reported by Cummer et al. (2013), in which the mean iCMC did not monotonically increase with peak current and, in fact, dropped for positive CG strokes above +150 kA. For negative strokes, only nine of them reached a value (absolute value) equal to or larger than 100 kA during the same time period. In comparison to thousands of positive sprites, negative sprites are sporadic (Barrington-Leigh et al., 1999; Taylor et al., 2008; Li et al., 2012; Lu et al., 2012; Lang et al., 2013; Boggs et al., 2016) in the literature, and the negative strokes with absolute peak current larger than 100 kA in the present study did not produce sprites.

A thunderstorm structure is an important factor for sprite initiation. The sounding data from Taiyuan at 2000 LST shown in Fig. 12 indicate that the environmental wind speed varied only slightly between 6 and 8 km; that is, the wind speed was about 9.77 m s^{-1} at 5.5 km and decreased to 8.23 m s^{-1} at 6.4 km, then increased back to 9.77 m s^{-1} at 7.0 km (similar value at about 7.44 km above ground level). Although the wind amplitude did not change significantly, the wind direction changed almost 90°, from nearly west at about 6 km to almost north at 8 km above ground level (the thundercloud moved from northwest to southeast). The existence of strong vertical wind shear in the region between 6 and 8 km typically leads to the formation of a tilted thunderstorm structure.

On the other hand, it is interesting to see that the vertical wind profile also shows that there was a large wind gradient (about 20 m s^{-1}) in the region between about 8 km and 12 km above ground level. In a normally charged thunder-

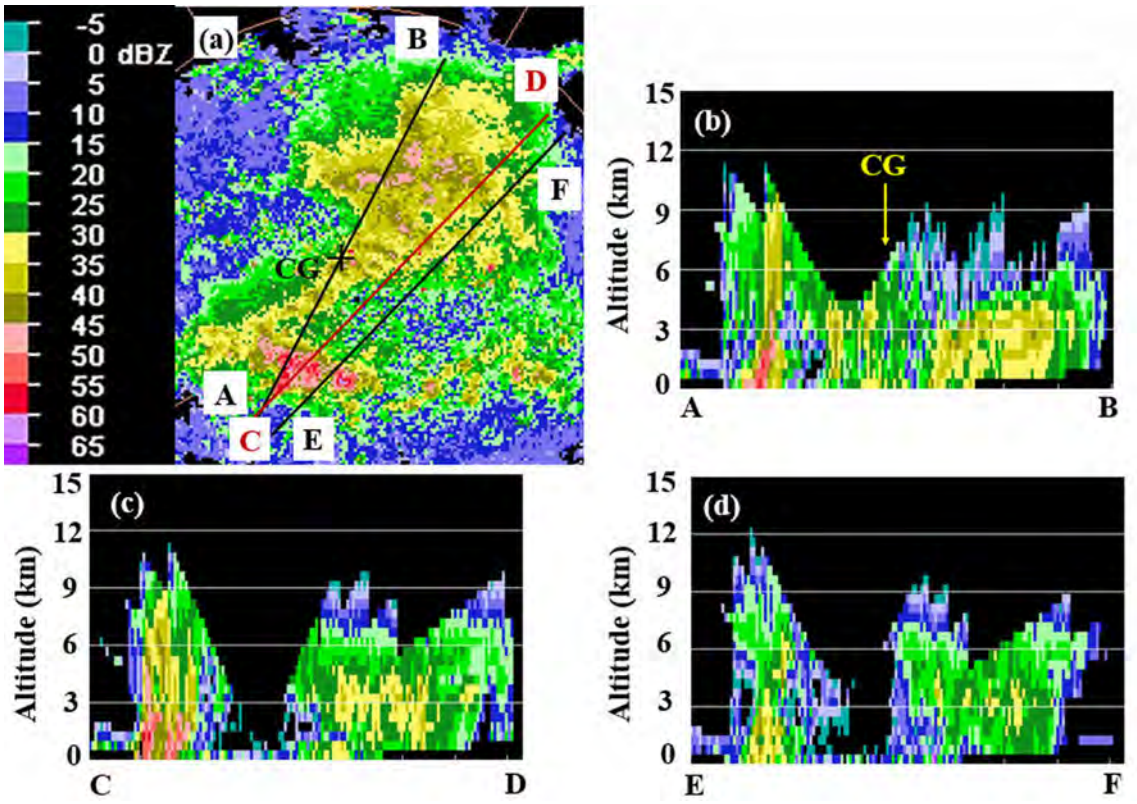

Fig. 9. Thunderstorm structure at 2242 LST. (a) Overlapped image of the parent flash with radar reflectivity. The parent flash for the sprite is marked by "+" and labeled with "CG" in the figure. The red line CD and black line EF are the same locations as lines 1 and 2, respectively, in Fig. 8a. (b–d) vertical cross sections along lines AB, CD, and EF in (a), respectively. The parent CG location is also shown in (b).

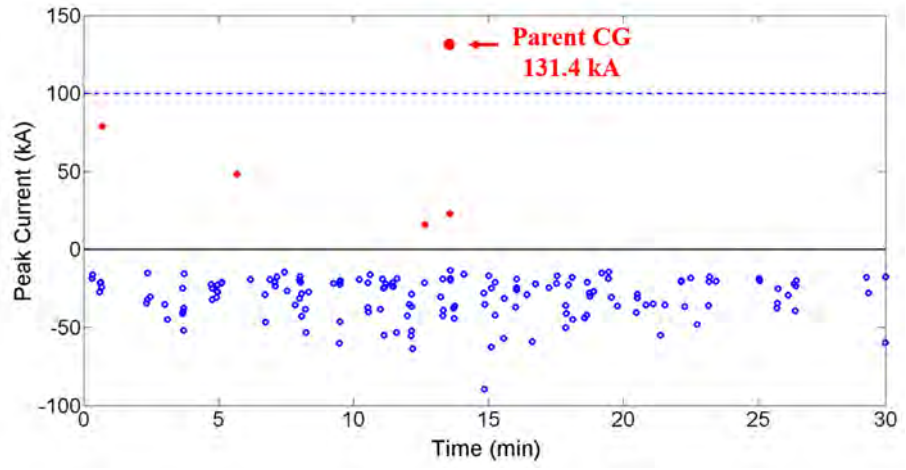

Fig. 10. A time scatter plot of the return stroke peak currents (within 50 km centered at the parent CG location) of CG lightning flashes within half an hour centered at the sprite. Red dots and blue circles represent positive strokes and negative ones, respectively. The parent CG for the sprite is also shown.

storm, ice crystals at upper altitudes (8–12 km) usually carry positive charges (Mansell et al., 2005; Saunders et al., 2006; Emersic and Saunders, 2010). Large wind shear in the 8–12 km region will cause the positive charges in the thunderstorm upper layer following a slanted path and moving to the stratiform region (Carey et al., 2005), thus having a closer distance from the ground than that in the anvil, providing favorable conditions for positive sprites production.

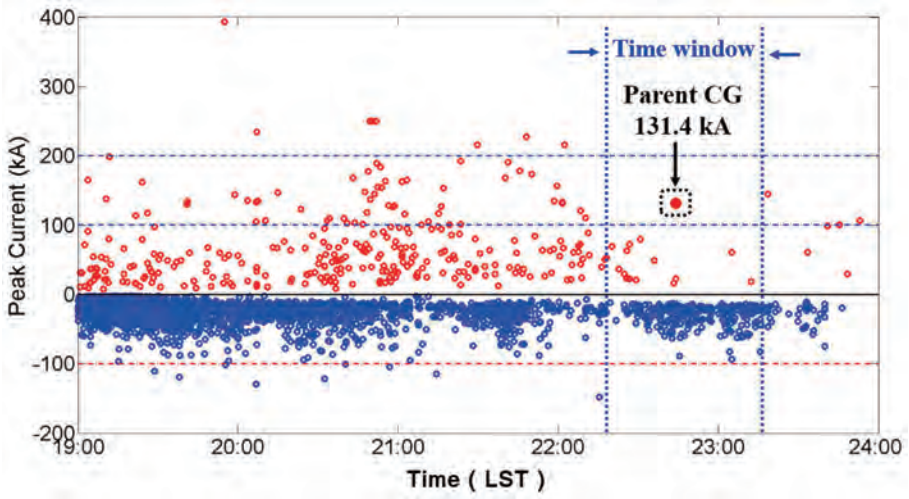

Fig. 11. A time scatter plot of the return stroke peak currents of the CG lightning flashes from 1900 to 2400 LST. Red dots and blue circles represent positive strokes and negative ones, respectively. The parent CG for the sprite is shown.

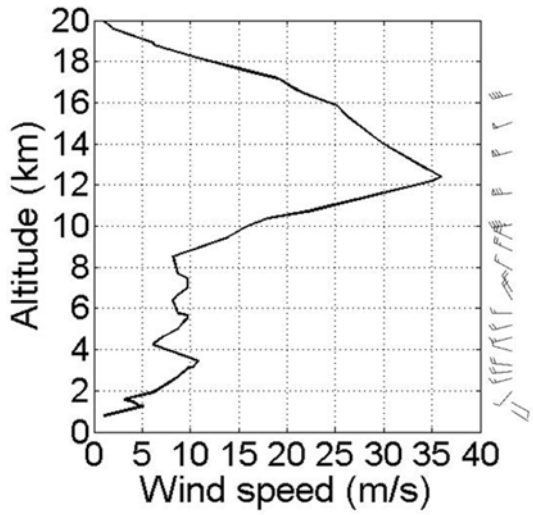

Fig. 12. Vertical wind profile from the Taiyuan sounding taken at 2000 LST 14 August 2012.

4. Conclusion

This paper presents a detailed analysis of an MCS that produced only one sprite during its whole evolution. Comprehensive analysis of the characteristics of the thunderstorm and lightning activity before, during, and after the sprite event was carried out using multiple data, including low-light level sprite imagery, and Doppler radar, lightning detection network, broadband magnetic field and sounding observations.

The results show that the recorded sprite was a long-delayed (38 ms) event containing only two elements that occurred in the continuous current process of the parent flash. The separation distance between the two elements was estimated to have been about 7.3 km (the actual horizontal displacement would be larger in three dimensions). The sprite was displaced horizontally about 20 km away from its parent CG. With an assumption of 50 km uncertainty in the parent CG location, the sprite bottom and top heights were about 57 ± 9 km and 78 ± 12 km, respectively, indicating the vertical extension of the sprite was not very large.

The parent CG was of positive polarity, with only one return stroke (peak current of 131.4 kA). The parent CG had the largest peak current among the CGs during the almost one-hour time window containing the sprite. The sprite occurred in a time interval during which the POP was not large (about 20%), and negative CGs dominated during the thunderstorm life cycle. The absolute value of the negative CG peak current during the same period was smaller than 100 kA and did not produce sprite.

Detailed analysis of the Doppler radar data showed that the maximum area of radar reflectivity ($\geqslant$10 dBZ) was small. The sprite did not occur in the time period during which the maximum area of the thunderstorm was reached. In the time window containing the sprite, the area with radar reflectivity larger than 40 dBZ decreased, and the area of reflectivity with 10–40 dBZ increased, suggesting that production of the sprite was related to the decay of the thunderstorm convection. No significant relationship between the sprite occurrence and the increase of the 30–35 dBZ and 35–40 dBZ interval was found. The large wind shear at 8–12 km altitude may have played an important role in the production of the sprite.

Acknowledgements. Special thanks are given to Michael SPLITT (msplitt@fit.edu) and Levi BOGGS (lboggs2014@my.fit.edu) for so many valuable discussions. This research was supported jointly by the National Natural Science Foundation of China (Grant Nos. 41374153 and 41574141), the High Resolution Earth Observation Funds for Young Scientists (Grant No. GFZX04060103-7-11) and the Youth Innovation Promotion Association of the Chinese Academy of Sciences (Grant No. 2013053). Special thanks will

also be given to the Xinglong Observatory, Chinese Academy of Sciences.

REFERENCES

Abarca, S. F., K. L. Corbosiero, and T. J. Galarneau Jr., 2010: An evaluation of the worldwide lightning location network (WWLLN) using the national lightning detection network (NLDN) as ground truth. *J. Geophys. Res.*, **115**, D18206, doi: 10.1029/2009JD013411.

Barrington-Leigh, C. P., U. S. Inan, M. Stanley, and A. S. Cummer, 1999: Sprites triggered by negative lightning discharges. *Geophys. Res. Lett.*, **26**(24), 3605–3608.

Boggs, L. D., N. Y. Liu, M. Splitt, S. Lazarus, C. Glenn, H. Rassoul, and S. A. Cummer, 2016: An analysis of five negative sprite-parent discharges and their associated thunderstorm charge structures. *J. Geophys. Res.*, **121**, 759–784, doi: 10.1002/2015JD024188.

Bovalo, C., C. Barthe, N. Yu, N. Yu, and N. Bègue, 2014: Lightning activity within tropical cyclones in the South West Indian Ocean. *J. Geophys. Res.*, **119**, 8231–8244, doi: 10.1002/2014JD021651.

Carey, L. D., M. J. Murphy, T. L. McCormick, and N. W. S. Demetriades, 2005: Lightning location relative to storm structure in a leading-line, trailing-stratiform mesoscale convective system, *J. Geophys. Res.*, **110**, D03105, doi: 10.1029/2003JD004371.

Chern, J. L., R. R. Hsu, H. T. Su, S. B. Mende, H. Fukunishi, Y. Takahashi, and L. C. Lee, 2003: Global survey of upper atmospheric transient luminous events on the ROCSAT-2 Satellite. *Journal of Atmospheric and Solar-Terrestrial Physics*, **65**(5), 647–659.

Cohen, M. B., U. S. Inan, R. K. Said, M. S. Briggs, G. J. Fishman, V. Connaughton, and S. A. Cummer, 2010: A lightning discharge producing a beam of relativistic electrons into space. *Geophys. Res. Lett.*, **37**, L18806, doi: 10.1029/2010GL044481.

Cummer, S. A., and W. A. Lyons, 2005: Implications of lightning charge moment changes for sprite initiation. *J. Geophys. Res.*, **110**, A04304, doi: 10.1029/2004JA010812.

Cummer, S. A., N. Jaugey, J. B. Li, W. A. Lyons, T. E. Nelson, and E. A. Gerken, 2006: Submillisecond imaging of sprite development and structure. *Geophys. Res. Lett.*, **33**, L04104, doi: 10.1029/2005gl024969.

Cummer, S. A., W. A. Lyons, and M. A. Stanley, 2013: Three years of lightning impulse charge moment change measurements in the United States. *J. Geophys. Res.*, **118**, 5176–5189, doi: 10.1002/jgrd.50442.

Cummins, K. L., M. J. Murphy, E. A. Bardo, W. L. Hiscox, R. B. Pyle, and A. E. Pifer, 1998: A combined TOA/MDF technology upgrade of the U.S. national lightning detection Network. *J. Geophys. Res.*, **103**(D8), 9035–9044.

Emersic, C., and C. P. R. Saunders, 2010: Further laboratory investigations into the relative diffusional growth rate theory of thunderstorm electrification. *Atmos. Res.*, **98**(2–4), 327–340.

Franz, R. C., R. J. Nemzek, and J. R. Winckler, 1990: Television image of a large upward electrical discharge above a thunderstorm system. *Science*, **249**(4964), 48–51.

Ganot, M., Y. Yair, C. Price, B. Ziv, Y. Sherez, E. Greenberg, A. Devir, and R. Yaniv, 2007: First detection of transient luminous events associated with winter thunderstorms in the eastern Mediterranean. *Geophys. Res. Lett.*, **34**, L12801, doi: 10.1029/2007GL029258.

Hardman, S. F., R. L. Dowden, J. B. Brundell, J. L. Bahr, Z. Kawasaki, and C. J. Rodger, 2000: Sprite observations in the northern territory of Australia. *J. Geophys. Res.*, **105**, 4689–4697.

Hsu, R. R., H. T. Su, A. B. Chen, L. C. Lee, M. Asfur, C. Price, and Y. Yair, 2003: Transient luminous events in the vicinity of Taiwan. Journal of Atmospheric and Solar-Terrestrial Physics, **65**(5), 561–566, doi: 10.1016/S1364-6826(02)00320-6.

Hu, W. Y., S. A. Cummer, W. A. Lyons, and T. E. Nelson, 2002: Lightning charge moment changes for the initiation of sprites. *Geophys. Res. Lett.*, **29**(8), 120-1–120-4, doi: 10.1029/2001GL014593.

Kuo, C. L., and Coauthors, 2007: Modeling elves observed by FORMOSAT-2 satellite. *J. Geophys. Res.*, **112**, A11312, doi: 10.1029/2007JA012407.

Kuo, C.-L., and Coauthors, 2009: Discharge processes, electric field, and electron energy in ISUAL-recorded gigantic jets. *J. Geophys. Res.*, **114**, A04314, doi: 10.1029/2008JA013791.

Lang, T. J., S. A. Cummer, S. A. Rutledge, and W. A. Lyons, 2013: The meteorology of negative cloud-to-ground lightning strokes with large charge moment changes: Implications for negative sprites. *J. Geophys. Res.*, **118**(14), 7886–7896.

Li, J., S. A. Cummer, W. A. Lyons, and T. E. Nelson, 2008: Coordinated analysis of delayed sprites with high-speed images and remote electromagnetic fields. *J. Geophys. Res.*, **113**, D20206, doi: 10.1029/2008JD010008.

Li, J. B., S. Cummer., G. P. Lu, and L. Zigoneanu, 2012: Charge moment change and lightning-driven electric fields associated with negative sprites and halos. *J. Geophys. Res.*, **117**, A09310, doi: 10.1029/2012JA017731.

Liu, N. Y., B. Kosar, S. Sadighi, J. R. Dwyer, and H. K. Rassoul, 2012: Formation of streamer discharges from an isolated ionization column at subbreakdown conditions. *Physical Review Letters*, **109**, 025002.

Liu, N. Y., M. G. McHarg, and H. C. Stenbaek-Nielsen, 2015a: High-altitude electrical discharges associated with thunderstorms and lightning. *Journal of Atmospheric and Solar-Terrestrial Physics*, **136**, 98–118, 10.1016/j.jastp.2015.05.013.

Liu, N. Y., N. Spiva, J. R. Dwyer, H. K. Rassoul, D. Free, and S. A. Cummer, 2015b: Upward electrical discharges observed above tropical depression dorian. *Nature Commun.*, **6**, 5995, doi: 10.1038/ncomms6995.

Liu, N. Y., J. R. Dwyer, H. C. Stenbaek-Nielsen, and M. G. McHarg, 2015c: Sprite streamer initiation from natural mesospheric structures. *Nature Commun.*, **6**, 7540, doi: 10.1038/ncomms8540.

Lu, G. P., S. A. Cummer, J. B. Li, F. Han, R. J. Blakeslee, and H. J. Christian, 2009: Charge transfer and in-cloud structure of large-charge-moment positive lightning strokes in a mesoscale convective system. *Geophys. Res. Lett.*, **36**, L15805, doi: 10.1029/2009GL038880.

Lu, G. P., S. A. Cummer, R. J. Blakeslee, S. Weiss, and W. H. Beasley, 2012: Lightning morphology and impulse charge moment change of high peak current negative strokes. *J. Geophys. Res.*, **117**, D04212, doi: 10.1029/2011JD016890.

Lu, G. P., and Coauthors, 2013: Coordinated observations of sprites and in-cloud lightning flash structure. *J. Geophys. Res.*, **118**, 6607–6632, doi: 10.1002/jgrd.50459.

Lyons, W. A., 1994: Characteristics of luminous structures in

the stratosphere above thunderstorms as imaged by low-light video. *Geophys. Res. Lett*., **21**(10), 875–878, doi: 10.1029/94 GL00560.

Lyons, W. A., 1996: Sprite observations above the U.S. High Plains in relation to their parent thunderstorm systems. *J. Geophys. Res*., **101**(D23), 29 641–29 652.

Lyons, W. A., T. E. Nelson, E. R. Williams, S. A. Cummer, and M. A. Stanley, 2003: Characteristics of sprite-producing positive cloud-to-ground lightning during the 19 July 2000 STEPS mesoscale convective systems. *Mon. Wea. Rev*., **131**, 2417–2427.

Mansell, E. R., D. R. MacGorman, C. L. Ziegler, and J. M. Straka, 2005: Charge structure and lightning sensitivity in a simulated multicell thunderstorm. *J. Geophys. Res*., **110**, D12101, doi: 10.1029/2004JD005287.

Neubert, T., T. H. Allin, H. Stenbaek-Nielsen, and E. Blanc, 2001: Sprites over Europe. *Geophys. Res. Lett*., **28**(18), 3585–3588.

Neubert, T., and Coauthors, 2005: Co-ordinated observations of transient luminous events during the EuroSprite2003 campaign. *Journal of Atmospheric and Solar-Terrestrial Physics*, **67**, 807–820, doi: 10.1016/j.jastp.2005.02.004.

Pan, L. X., X. S. Qie, D. X. Liu, D. F. Wang, and J. Yang, 2009: The lightning activities in super typhoons over the Northwest Pacific. *Science China Earth Sciences*, **53**(8), 1241–1248.

Pasko, V. P., 2007: Red sprite discharges in the atmosphere at high altitude: The molecular physics and the similarity with laboratory discharges. *Plasma Sources Science and Technology*, **16**, S13–S29, doi: 10.1088/0963-0252/16/1/S02.

Pasko, V. P., U. S. Inan, T. F. Bell, and Y. N. Taranenko, 1997: Sprites produced by quasi-electrostatic heating and ionization in the lower ionosphere. *J. Geophys. Res*., **102**(A3), 4529–4561, doi: 10.1029/96JA03528.

Pinto, O. Jr., and Coauthors, 2004: Thunderstorm and lightning characteristics associated with sprites in Brazil. *Geophys. Res. Lett*., **31**, L13103, doi: 10.1029/2004GL020264.

Qin, J. Q., S. Celestin., and V. P. Pasko, 2012: Minimum charge moment change in positive and negative cloud to ground lightning discharges producing sprites. *Geophys. Res. Lett*., **39**, L22801, doi: 10.1029/2012GL053951.

São Sabbas, F. T., and D. D. Sentman, 2003: Dynamical relationship of infrared cloudtop temperatures with occurrence rates of cloud-to-ground lightning and sprites. *Geophys. Res. Lett*., **30**(5), 1236. doi: 10.1029/2002GL015382.

Sato, M., and Coauthors, 2015: Overview and early results of the global lightning and sprite measurements mission. *J. Geophys. Res*., **120**(9), 3822–3851, doi: 10.1002/2014JD022428.

Sato, M., and Coauthors, 2016: Horizontal distributions of sprites derived from the JEM-GLIMS nadir observations. *J. Geophys. Res*., **121**, 3171–3194.

Saunders, C. P. R., H. Bax-Norman, C. Emersic, E. E. Avila, and N. E. Castellano, 2006: Laboratory studies of the effect of cloud conditions on graupel/crystal charge transfer in thunderstorm electrification. *Quart. J. Roy. Meteor. Soc*., **132**(621), 2653–2673.

Sentman, D. D., E. M. Wescott, D. L. Osborne, D. L. Hampton, and M. J. Heavner, 1995: Preliminary results from the Sprites94 aircraft campaign: 1. Red sprites. *Geophys. Res. Lett*., **22**(10), 1205–1208.

Sonnenfeld, R. G., and W. W. Hager, 2013: Electric field reversal in sprite electric field signature. *Mon. Wea. Rev*., **141**, 1731–1735.

Soula, S., O. van der Velde, J. Montanyà, T. Neubert, O. Chanrion, and M. Ganot, 2009: Analysis of thunderstorm and lightning activity associated with sprites observed during the EuroSprite campaigns: Two case studies. *Atmos. Res.*, **91**, 514–528.

Soula, S., and Coauthors, 2015: Time and space correlation between sprites and their parent lightning flashes for a thunderstorm observed during the HyMeX campaign. *J. Geophys. Res*., **120**, 11 552–11 574, doi: 10.1002/2015JD023894.

Stanley, M., M. Brook, P. Krehbiel, and S. A. Cummer, 2000: Detection of daytime sprites via a unique sprite ELF signature. *Geophys. Res. Lett*., **27**(6), 871–874.

Su, H. -T., R. -R. Hsu, A. B. -C. Chen, Y. -J. Lee, and L. -C. Lee, 2002: Observation of sprites over the Asian continent and over oceans around Taiwan. *Geophys. Res. Lett*., **29**(4), 3-1–3-4, doi: 10.1029/2001GL013737.

Taylor, M. J., and Coauthors, 2008: Rare measurements of a sprite with halo event driven by a negative lightning discharge over Argentina. *Geophys. Res. Lett*., **35**, L14812, doi: 10.1029/2008GL033984.

van der Velde, O. A., Á. Mika, S. Soula, C. Haldoupis, T. Neubert, and U. S. Inan, 2006: Observations of the relationship between sprite morphology and in-cloud lightning processes. *J. Geophys. Res*., **111**, D15203, doi: 10.1029/2005JD006879.

van der Velde, O. A., W. A. Lyons, T. E. Nelson, S. A. Cummer, J. B. Li, and J. Bunnell, 2007: Analysis of the first gigantic jet recorded over continental North America. *J. Geophys. Res*., **112**, D20104, doi: 10.1029/2007JD008575.

Williams, E., E. Downes, R. Boldi, W. Lyons, and S. Heckman, 2007: Polarity asymmetry of sprite-producing lightning: A paradox? *Radio Sci*., **42**, RS2S17, doi: 10.1029/2006 RS003488.

Williams, E., and Coauthors, 2012: Resolution of the sprite polarity paradox: The role of halos. *Radio Sci*., **47**, RS2002, doi: 10.1029/2011RS004794.

Winckler, J. R., W. A. Lyons, T. E. Nelson, and R. J. Nemzek, 1996: New high-resolution ground-based studies of sprites. *J. Geophys. Res*., **101**(D3), 6997–7004, doi: 10.1029/95JD 03443.

Yang, J., X. S. Qie, G. S. Zhang, Y. Zhao., and T. Zhang, 2008: Red sprites over thunderstorms in the coast of Shandong province, China. *Chinese Science Bulletin*, **53**(7), 1079–1086.

Yang, J., X. S. Qie., G. L. Feng, 2013a: Characteristics of one sprite-producing summer thunderstorm. *Atmos. Res*, **127**, 90–115.

Yang, J., X. S. Qie, C. Chao, and G. L. Feng, 2013b: Case studies of sprite-producing and non-sprite-producing summer thunderstorms. *Adv. Atmos. Sci*., **30**(6), 1786–1808, doi: 10.1007/s00376-013-2120-5.

Yang, J., G. P. Lu, L. -J. Lee, and G. L. Feng, 2015: Long-delayed bright dancing sprite with large Horizontal displacement from its parent flash. *Journal of Atmospheric and Solar-Terrestrial Physics*, **129**, 1–5, doi: 10.1016/j.jastp.2015.04.001.

Zhang, Y. J., and Coauthors, 2014: Experiments of artificially triggered lightning and its application in Conghua, Guangdong, China. *Atmos. Res.*, **135–136**, 330–343, doi.org/10.1016/j.atmosres.2013.02.010.